Computers in Biology and Medicine 164 (2023) 107294

Contents lists available at ScienceDirect

Computers in Biology and Medicine

journal homepage: www.elsevier.com/locate/compbiomed

Modelling smart drug release with functionally graded materials

Gabriella Bretti [a], Sean McGinty [b], Giuseppe Pontrelli [a,*]

[a] Istituto per le Applicazioni del Calcolo – CNR, Via dei Taurini 19 00185 Rome, Italy
[b] Division of Biomedical Engineering, University of Glasgow, Glasgow, UK

ARTICLE INFO

Keywords:
Drug delivery
Smart materials
Mathematical models
Numerical methods

ABSTRACT

Functionally graded materials (FGMs), possessing properties that vary smoothly from one region to another, have been receiving increasing attention in recent years, particularly in the aerospace, automotive and biomedical sectors. However, they have yet to reach their full potential. In this paper, we explore the potential of FGMs in the context of drug delivery, where the unique material characteristics offer the potential of fine-tuning drug-release for the desired application. Specifically, we develop a mathematical model of drug release from a thin film FGM, based upon a spatially-varying drug diffusivity. We demonstrate that, depending on the functional form of the diffusivity (related to the material properties) a wide range of drug release profiles may be obtained. Interestingly, the shape of these release profiles are not, in general, achievable from a homogeneous medium with a constant diffusivity.

1. Introduction

Technological advances over the past decades have led to the development of sophisticated drug delivery devices (DDDs) that enable targeting and control of drug delivery [1]. Important examples include drug-eluting stents for the treatment of coronary artery disease, capsules for the delivery of drug across several applications and antibiotic-eluting orthopaedic implants to combat post-surgical infection, to name but a few [2–4]. The drug is usually contained within one or more materials, often polymers, whose properties ultimately dictate how the drug is released. Better control of the drug release is often desired and many new technologies are being developed to try to address this [5]. In most cases, maintaining local drug concentrations in the biological environment within a therapeutic range is desirable, while most DDDs deliver a *burst* of drug (i.e. almost all drug delivered over a short period of time) followed by more sustained release over a longer period. This can lead to intervals of time where (i) toxic and/or (ii) sub-therapeutic concentrations are achieved if the drug release is not tailored appropriately. Technologies that enable fine-tuning of the drug release properties would fill this gap, particularly as we move into an era of personalized medicine.

Among the possible concurrent physical processes, such as dissolution, polymer swelling and degradation, diffusion remains a key (and often the dominant) mechanism used to control the release rate from DDDs. Indeed, there is an abundance in the literature of mathematical models focussing on diffusion-controlled DDDs [6,7]. These typically describe diffusion of drug from a homogeneous single-layered platform, with an associated constant effective diffusion coefficient [8]. However, there are also several models that consider diffusion within heterogeneous multi-layer materials, exhibiting a different constant diffusivity in each layer [9,10], deriving from differing properties such as polymer type/composition, or varying levels of porosity [11]. Stimuli-responsive DDDs are another class of DDDs that control the release of drug in response to external triggers such as temperature, pH and many others [12,13]. In these systems, the effectiveness of delivery can be improved by designing structures capable of responding to specific conditions by altering their properties and favouring the selective release of the loaded drug. However, to the best of our knowledge, a comprehensive investigation of diffusion-based drug release from a continuous non-homogeneous medium is lacking. This is despite growing interest in continuous non-homogeneous materials in many areas of science [14].

Recently, much attention has been paid to functionally graded materials (FGMs), a variety of composite media in which the constitutive properties vary smoothly and continuously from one surface to another. This is in contrast to more common approaches for achieving varying material structure, such as layer-by-layer assembly, where there is an abrupt change in properties from one layer to the next (Fig. 1). FGMs, i.e. materials that have a progressive compositional gradient changing from one side to the other, are already being used in a wide range of applications [15–17]. They have primarily been used in engineering and material science, with the purpose to relax the internal thermal stress at elevated temperatures [18]. FGMs have already shown promise in a number of applicative fields, including the aerospace, automotive,

* Corresponding author.
E-mail address: giuseppe.pontrelli@gmail.com (G. Pontrelli).

https://doi.org/10.1016/j.compbiomed.2023.107294
Received 20 April 2023; Received in revised form 6 July 2023; Accepted 28 July 2023
Available online 31 July 2023

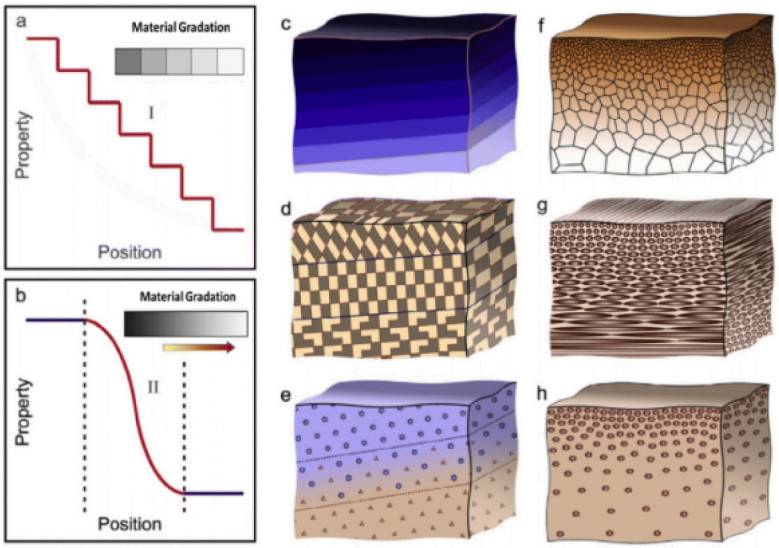

Fig. 1. Schematic showing (a,c,d,e) a multi-layered medium with step-wise properties versus a functionally graded material (b,f,g,h) with continuously varying material characteristics [11].

tissue engineering and biomedical sectors [15,19], but have yet to reach their full potential. In this context, new possibilities are derived from 3D printing technology to manufacture smart materials having graded micro-porosity and density [20]. However, despite today's capabilities in micro-engineering technology, FGMs do not appear to have been considered for fine-tuning drug release [17].

In this paper, through a mathematical mechanistic model and a simulation approach, we explore the potential of FGMs as a new class of controlled drug delivery materials, in the attempt to establish whether varying material properties can provide an advantage over a homogeneous medium. We develop a continuum model to describe drug transport within, and release from, a thin film FGM which exhibits a spatially-dependent drug diffusivity. A numerical solution is derived and results are presented for several different spatially-dependent diffusivity functional forms. Comparisons are made between resulting drug concentration and release profiles.

2. Methodology

2.1. Formulation of the problem

Consider a thin film FGM whose properties vary smoothly and continuously across its thickness L (Fig. 2). Assuming drug transport is governed by diffusion, and neglecting edge effects, we describe transport of drug via the diffusion equation, with a spatially dependent diffusion coefficient $D(x)$:

$$\frac{\partial c}{\partial t} = \frac{\partial}{\partial x}\left(D(x)\frac{\partial c}{\partial x}\right), \qquad x \in [0, L], \quad t \in [0, T], \tag{2.1}$$

where $c(x,t)$ is the volume-averaged concentration of drug. Given the continuously varying nature of the material and the common desire to control a large burst release, we assume a monotonically decreasing functional form for $D(x)$ ranging from D_{max} at $x = 0$ to D_{min} at $x = L$. While, in principle, a FGM may be manufactured to exhibit diffusion properties satisfying any such spatial-dependence, we choose as our baseline case a logistic function of the form

$$D(x) = D_{max} - (D_{max} - D_{min})\frac{1}{1 + e^{-\lambda(x-\sigma)}}, \tag{2.2}$$

where $\lambda \geq 0$ [cm^{-1}] is inversely related to the width of the transition layer, and $\sigma \in [0, L]$ [cm] denotes the location of the transition centre.

Through the many combinations of parameters λ and σ, the function (2.2) can describe a variety of different material properties and configurations. For example, the case of a homogeneous medium with constant diffusion coefficient at the midpoint of the two extreme values is recovered for $\lambda = 0$, while a two-layer substrate with a diffusivity jump from D_{max} to D_{min} at σ is recovered for $\lambda \to \infty$. For simplicity, a constant initial drug concentration, C_0, is considered. At $x = 0$, a zero-flux condition is imposed, mimicking the typical case where the drug-containing material is applied as a coating over an impermeable platform, while at $x = L$ (contact with the release medium) a perfect sink condition is imposed (Fig. 2), replicating typical in-vitro drug release experiments and in-vivo scenarios where the material is in contact with a relatively large volume of fluid:

$$c(x, 0) = C_0, \qquad x \in [0, L], \tag{2.3}$$

$$-D(0)\frac{\partial c}{\partial x}(0, t) = 0, \qquad t \in [0, T], \tag{2.4}$$

$$c(L, t) = 0, \qquad t \in [0, T]. \tag{2.5}$$

In addition to the logistic function, many other choices for $D(x)$ ranging from a maximum value D_{max} to a minimum D_{min} are possible, and we also consider as three further examples, a power-law, a trigonometric and an exponential form:

$$D(x) = D_{max} - (D_{max} - D_{min})x^{\alpha}, \tag{2.6}$$

$$D(x) = D_{min} + (D_{max} - D_{min})\left(\frac{\arccos(2x-1)}{\pi}\right)^{\theta}, \tag{2.7}$$

$$D(x) = D_{max}\exp\left(-\ln\left(\frac{D_{max}}{D_{min}}\right)x^{\gamma}\right). \tag{2.8}$$

parametrized by $\alpha, \theta, \gamma > 0$ (FGM parameters), respectively. With these choices, sharp diffusivity variations and changes of concavity are possible, depending on the selected parameters.

2.2. Modelling drug release from a FGM

Eqs. (2.1)–(2.5) are non-dimensionalized via

$$x \to \frac{x}{L}; \qquad t \to \frac{D^*}{L^2}t; \qquad T \to \frac{D^*}{L^2}T; \qquad \lambda \to \lambda L; \qquad \sigma \to \frac{\sigma}{L};$$
$$D(x) \to \frac{D(x)}{D^*}; \qquad c \to \frac{c}{C_0},$$

where $D^* \in [D_{min}, D_{max}]$ is a reference value for the diffusivity, chosen to be one order of magnitude higher than D_{min} and one order of magnitude lower than D_{max} (Table 1).

Fig. 2. Schematic representation of a thin film FGM drug release system (shaded green) in contact on one side with an impermeable backing and on the other by release medium. The arrow represents the direction of the mass flux (figure not to scale).

This gives rise to the following non-dimensional model

$$\frac{\partial c}{\partial t} = \frac{\partial}{\partial x}\left(D(x)\frac{\partial c}{\partial x}\right), \qquad x \in [0,1],\ t \in [0,T], \tag{2.9}$$

$$c(x,0) = 1, \qquad x \in [0,1], \tag{2.10}$$

$$D(0)\frac{\partial c}{\partial x}(0,t) = 0, \qquad t \in [0,T], \tag{2.11}$$

$$c(1,t) = 0, \qquad t \in [0,T], \tag{2.12}$$

where

$$D(x) = D_{max} - (D_{max} - D_{min})\frac{1}{1+e^{-\lambda(x-\sigma)}}, \tag{2.13}$$

and the functions (2.6), (2.7), (2.8) are non-dimensionalized similarly.

The drug release profile, P_r, the cumulative mass of drug released over time, is a key quantity measured by experimentalists to explore how changes in DDD design impact the rate of drug release. This may be calculated from the model via

$$P_r(t) = \left(1 - \frac{M(t)}{M_0}\right) \times 100, \ t \in [0,T], \tag{2.14}$$

where $M(t)$ is the time-varying non-dimensional mass of drug in the FGM, taking the initial value $M_0 = 1$:

$$M(t) = \int_0^1 c(x,t)dx, \qquad t \in [0,T], \quad M(0) = 1. \tag{2.15}$$

Eq. (2.14) allows one to explore how variations in model parameter values would theoretically influence the drug delivery, in principle enabling one to optimize the FGM design to achieve a target drug release profile for a given application. Here, we are particularly interested in comparing the release profiles that are obtained from a homogeneous material (constant diffusion coefficient) with those obtained from a FGM (space-varying diffusion coefficient).

2.3. Numerical method

Eqs. (2.9)–(2.12) are solved numerically by considering a meshgrid with equispaced nodes $x_i := i\Delta x$, $i = 0,\dots,M$ with $\Delta x = 10^{-2}$ for the discretization of $[0,1]$. The time discretized points in $[0,T]$ are taken as $t_n := n\Delta t, n = 0,\dots,N$. The model parameters are reported in Table 1. Following [21], we approximate Eq. (2.9) with a finite difference scheme obtained by means of Taylor expansions:

$$\Delta_i(D,c) := \frac{(D_i + D_{i+1})(c_{i+1} - c_i) - (D_{i-1} + D_i)(c_i - c_{i-1})}{2\Delta x^2}, \tag{2.16}$$

giving rise to

$$c_i^{n+1} = c_i^n + \Delta t\Delta_i(D^n, c^n), \ i = 1,\dots,M-1, \quad n = 0,\dots,N, \tag{2.17}$$

where c_i^n denotes $c(x_i,t_n)$. The stability condition $\Delta t \le \frac{\Delta x^2}{2\max D(x)}$ is imposed. The above scheme reduces to the classical explicit finite difference method for D constant. A second order approximation [22] for the Neumann boundary condition at $x_0 = 0$ and perfect sink condition at $x_M = 1$ are applied for Eqs. (2.11)–(2.12), respectively:

$$c_0^{n+1} = \frac{4}{3}c_1^{n+1} - \frac{1}{3}c_2^{n+1}, \ n = 0,\dots,N, \tag{2.18}$$

$$c_M^{n+1} = 0, \qquad n = 0,\dots,N. \tag{2.19}$$

Table 1
Physical and numerical parameters of the problem. For the purposes of this study, L is chosen to be representative of a thin drug-eluting stent coating, while $[D_{min}, D_{max}]$ covers a range of typical drug diffusion coefficients within stent coatings reported in the literature [23,24].

Parameter	Description	Value [dim.]	Value [non-dim.]
L	Coating thickness [23,24]	$5 \cdot 10^{-4}$ cm	1
D_{max}	Max. diffusivity	10^{-11} cm^2/s	10
D_{min}	Min. diffusivity	10^{-13} cm^2/s	0.1
D^*	Reference diffusivity [23,24]	10^{-12} cm^2/s	1
T	Max. time	30 days	10.4
C_0	Initial concentration	0.5 mol/cm^3	1
Δx	Space step	$5 \cdot 10^{-6}$ cm	10^{-2}
Δt	Time step	1.25 s	$5 \cdot 10^{-6}$

All the simulations are implemented in Matlab©. We compute the approximate mass M by the composite rectangle rule:

$$M(t_n) = \Delta x \sum_{i=0}^{M} c_i^n, \quad n = 0,\dots,N. \tag{2.20}$$

3. Results

3.1. Case A: constant D

While the numerical method described above is, in general, required for a spatially-varying diffusivity, the problem with constant diffusion coefficient may be solved analytically by separation of variables, providing the non-dimensional exact solution [25]:

$$c(x,t) = \sum_{j=0}^{\infty} a_j \cos(\lambda_j x)\exp(-\lambda_j^2 D\, t), \tag{3.1}$$

with the eigenvalues $\lambda_j = \pi\left(j + \frac{1}{2}\right)$, $j = 0,1,2\dots$, and the coefficients:

$$a_j = 2\int_0^1 \cos(\lambda_j x)dx = (-1)^j \frac{4}{\pi(2j+1)}.$$

The corresponding exact solution for the non-dimensional drug mass is written as:

$$M(t) = \int_0^1 c(x,t)dx = \sum_{j=0}^{\infty} \frac{a_j^2}{2}\exp(-\lambda_j^2 D\, t), \quad \text{for all } t \in [0,T], \tag{3.2}$$

and the drug release profile is obtained by Eq. (2.14). By comparing the exact solution with the numerical approximation in the above section, we are able to validate the numerical scheme. In practice, the series (3.1) is truncated at a finite number of terms, J, with $J = 10$ found to be sufficient to guarantee good accuracy at all times. Here, $D = 1$ is chosen for the purposes of the comparison. In Fig. 3 (left) the exact solution given by Eq. (3.1) and the approximate solution given by the numerical solution of Eqs. (2.9)–(2.12) are depicted at three times. The corresponding drug release profiles are shown on the right panel. The agreement is excellent, providing confidence in the accuracy of the numerical scheme.

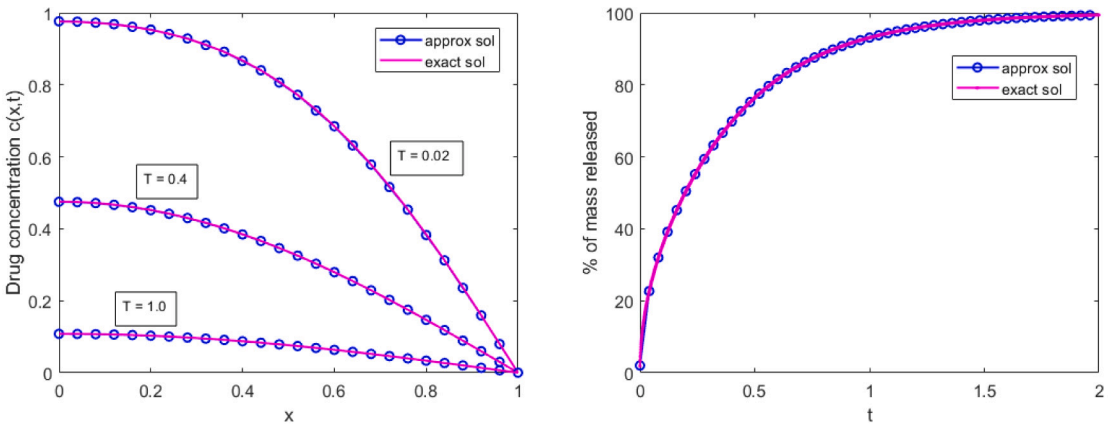

Fig. 3. Left: Nondimensional concentration profiles at three times, with exact (3.1) vs. the approximate solution obtained by the numerical scheme (2.17)–(2.19) with constant $D = 1$. Right: Corresponding exact and approximated drug release profiles computed using (2.14) with the exact mass in Eq. (3.2) and its numerical approximation in Eq. (2.20).

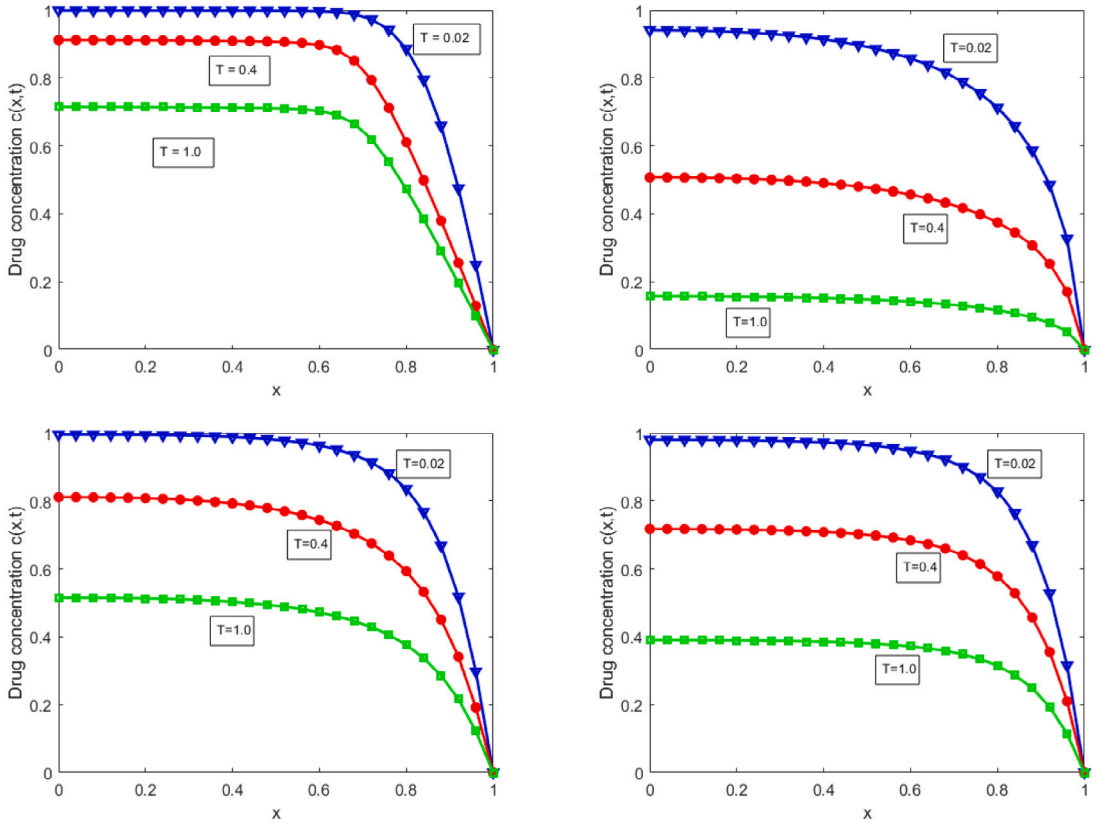

Fig. 4. Nondimensional drug concentration profiles at three times. Top left: Logistic function (2.13) ($\lambda = 25, \sigma = 0.5$). Top right: Power-law function (2.6) ($\alpha = 0.5$). Bottom left: Arccos function (2.7) ($\theta = 3$). Bottom right: Exponential function (2.8) ($\gamma = 2$).

3.2. Case B: variable $D(x)$

Fig. 4 compares the spatial drug concentration profiles within the FGM at three different times, for the logistic, power-law, arccos and exponential forms of $D(x)$. This figure demonstrates that, differently from a multi-layer configuration, where a concentration jump may be possible at the interfaces, the concentration is a continuous decreasing function in space. However, while in all cases a steep gradient is observed near the release medium $x = 1$, where a sink condition is imposed, the drug is retained differently depending on the form of $D(x)$ related to the FGM properties.

In Fig. 5 we present the results obtained with the logistic diffusivity function $D(x)$ defined in (2.13). We start by fixing $\sigma = 0.5$ and varying λ in the range $\lambda \in \{15, 25, 50\}$. Fig. 5 (left) displays $D(x)$, while Fig. 5 (right) shows the corresponding drug release profiles. The spatial distribution gives rise to varying drug release profiles. In particular, the release rate increases with decreasing λ, giving rise to quicker overall drug delivery.

Next, we fix $\lambda = 50$ and vary σ in the range $\sigma = 0.5, 0.7, 0.8$, with Fig. 6 (left) displaying $D(x)$, and 6 (right) displaying % of mass released. We observe that increasing σ (moving the transition centre closer to the release medium) results in quicker release. This is explained because the higher diffusivity region occupies a larger portion of the thin film. Taken together, the results in Figs. 5–6 demonstrate the tunability of the drug release profile by varying model parameters, in other words, by varying the underlying FGM properties. Figs. 7–9 show the corresponding results for the other functional forms of $D(x)$

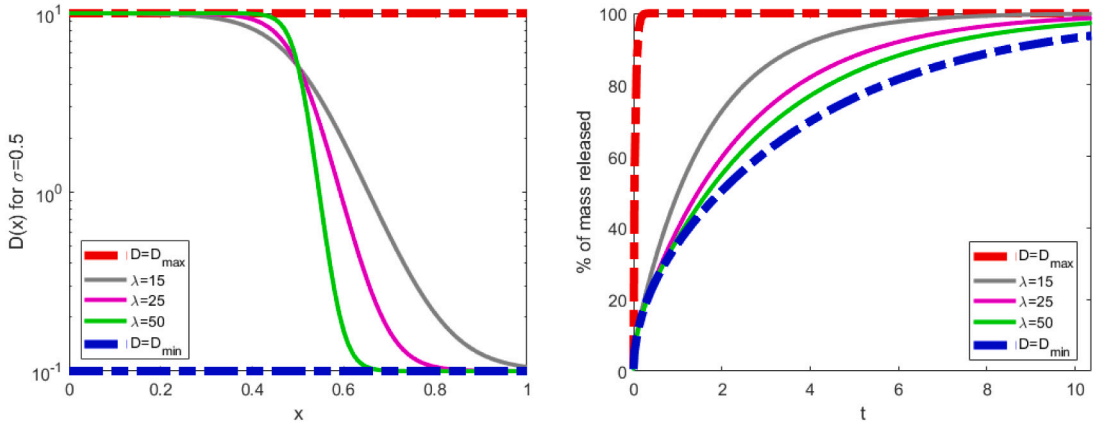

Fig. 5. Variable diffusion functions $D(x)$ as in Eq. (2.13) for $\sigma = 0.5$ and $\lambda = 15, 25, 50$ (left). Corresponding drug release profiles (right).

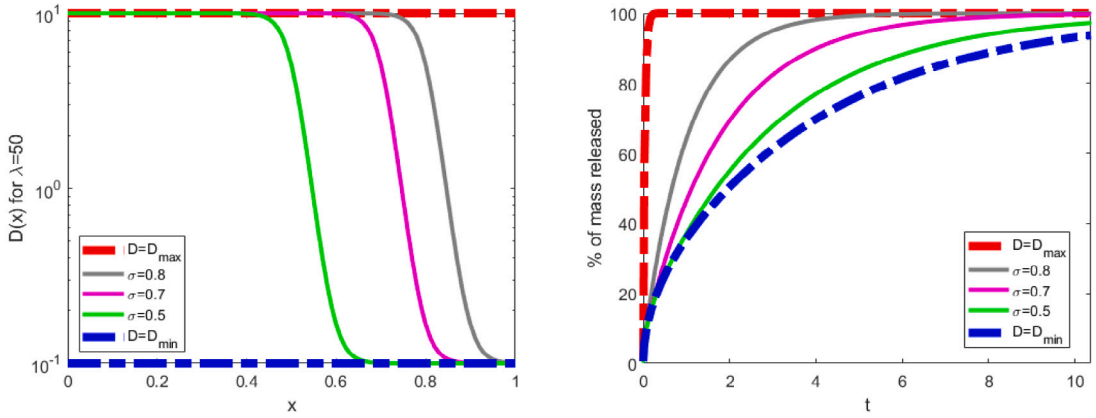

Fig. 6. Variable diffusion functions $D(x)$ as in Eq. (2.13) for $\lambda = 50$ fixed, $\sigma = 0.5, 0.7, 0.8$ (left). Corresponding drug release profiles (right).

considered: power law (7), Arccos (8) and exponential (9). Although the release curves are always enclosed between the corresponding curves for the limit cases $D = D_{min}$ and $D = D_{max}$, a wide spread of drug release profiles obtainable by varying model (FGM) parameters is observable.

To quantitatively compare the various cases, in Table 2 we compute three indices: the time taken for (i) 50% release (T_{50}) and (ii) 95% release (T_{95}) and (iii) the % of drug released at an arbitrary early time ($P_r^{t=0.5}$), with the last of these being indicative of the initial drug release rate. The corresponding values for the limiting cases of homogeneous materials with constant $D = D_{min}$ and $D = D_{max}$ are reported in the first two lines. For the power law model, increasing the parameter α, reduces T_{50} and T_{95} while increasing $P_r^{t=0.5}$. For the Arccos model, decreasing θ reduces T_{50} and T_{95} while increasing $P_r^{t=0.5}$. Finally, for the exponential model, increasing γ reduces T_{50} and T_{95} while increasing $P_r^{t=0.5}$.

At first glance, the drug release profiles in Figs. 5–9 may appear similar in shape and typical of those resulting from linear diffusion problems. This begs the question of whether it is worth the effort developing a complicated FGM with a varying $D(x)$ if a homogeneous material with a constant D could also achieve the same drug release profile. To probe this, we checked whether the drug release profiles for the various $D(x)$ were proportional to $\sqrt{t}$ for sufficiently 'small times': for Fickian diffusion, indeed, it can be shown that the $\sqrt{t}$ relationship is valid for $P_r \leq 60\%$, see [26]. We found that, in general, this relationship was not satisfied across the different functional forms for $D(x)$ considered. Assuming $P_r = Kt^{\beta}$, we inversely estimated the best-fitting K and β for a subset of the cases considered (Figs. 10–11), finding that exponents of t giving rise to a linear drug release profile varied from around 0.5–0.7 (Table 3). This demonstrates that the variety of shape of profiles obtained with an FGM cannot, in general, be obtained with a homogeneous material.

Table 2
Characteristic release times for FGMs having the same extreme values $D_{min} = 0.1$ and $D_{max} = 10$, but different forms of $D(x)$.

	Parameters	time for 50% release (T_{50})	time for 95% release (T_{95})	% release at $t = 0.5$ ($P_r^{t=0.5}$)
D_{min}	–	2.0	11.0	25.22
D_{max}	–	0.02	0.12	100
logistic (2.13)	$\lambda = 15, \sigma = 0.5$	1.02	4.81	31.62
	$\lambda = 15, \sigma = 0.7$	0.30	1.21	71.52
	$\lambda = 15, \sigma = 0.8$	0.12	0.43	96.98
	$\lambda = 50, \sigma = 0.5$	1.72	8.93	25.42
	$\lambda = 50, \sigma = 0.7$	1.11	5.50	29.33
	$\lambda = 50, \sigma = 0.8$	0.72	3.13	41.32
power-law (2.6)	$\alpha = 0.1$	0.81	4.02	36.58
	$\alpha = 0.5$	0.34	1.62	63.18
	$\alpha = 3$	0.11	0.45	96.24
arccos (2.7)	$\theta = 5$	1.53	7.51	26.42
	$\theta = 3$	0.82	3.87	36.24
	$\theta = 1$	0.10	0.48	95.76
exponential (2.8)	$\gamma = 0.5$	1.28	6.40	28.83
	$\gamma = 2$	0.64	3.00	42.66
	$\gamma = 10$	0.19	0.85	83.09

4. Conclusions

This study has presented a theoretical model of drug release from a thin film DDD, assuming spatially-varying diffusion to be the dominant transport mechanism. Several different functional forms have been

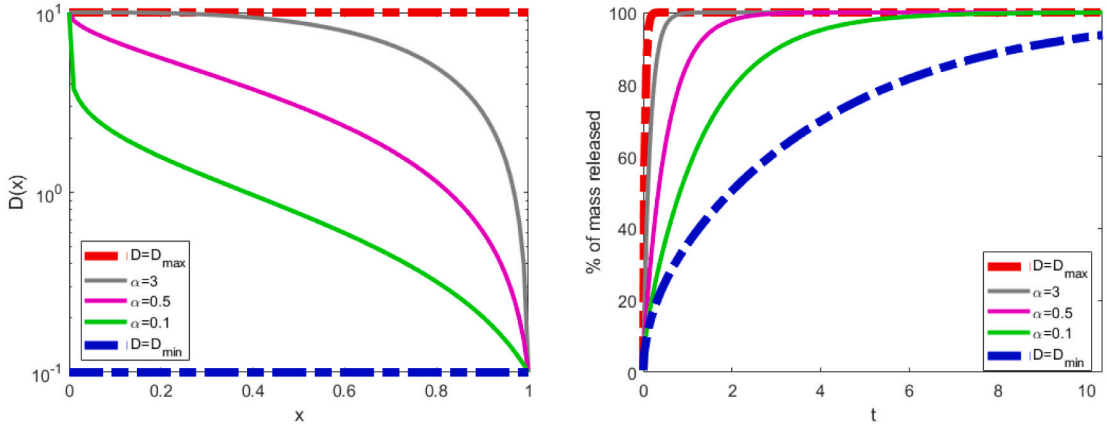

Fig. 7. Power-law diffusivity functions as in Eq. (2.6) for three values of α (left). Corresponding release profiles (right).

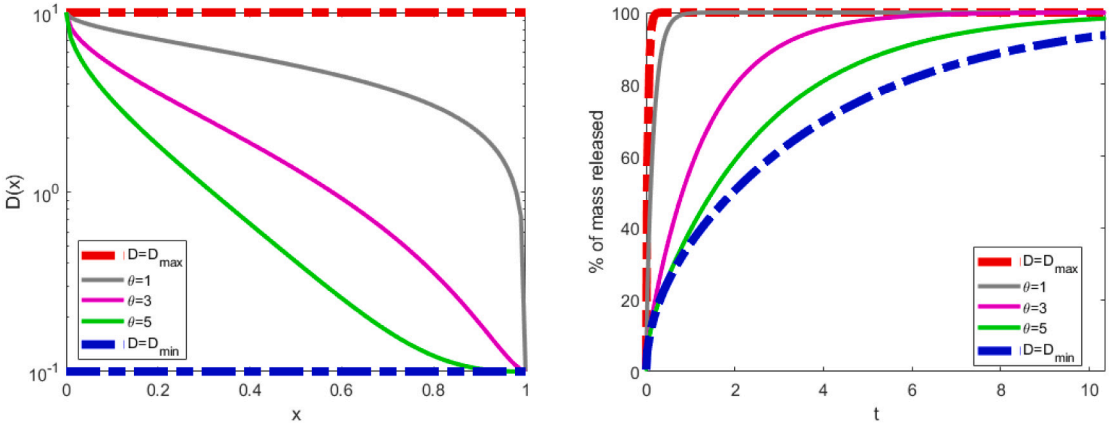

Fig. 8. Arccos diffusion functions $D(x)$ as in Eq. (2.7) for three values of θ (left). Corresponding release profiles (right).

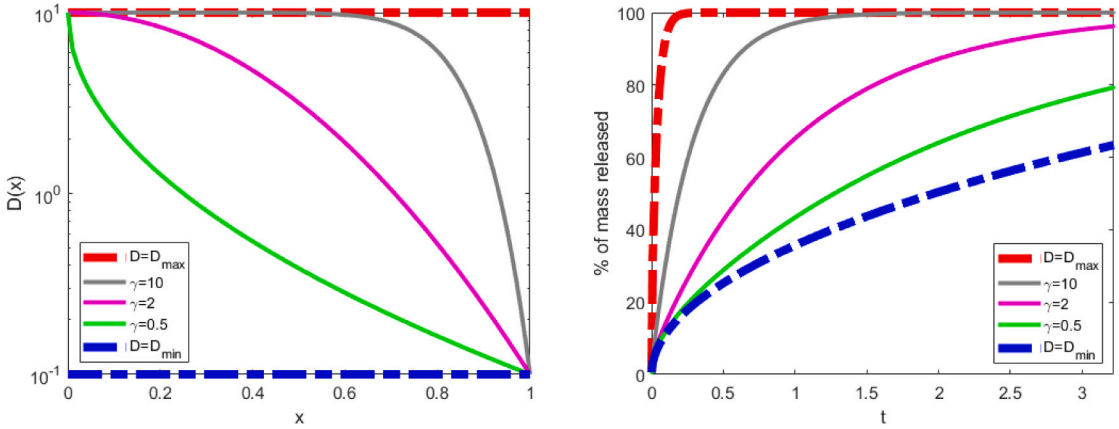

Fig. 9. Exponential diffusion functions $D(x)$ as in Eq. (2.8) for three values of γ (left). Corresponding release profiles (right).

considered for the diffusivity. The results show that a wide range of drug release profiles can be obtained by varying the material shape and, moreover, by varying the parameters within each functional form. This work demonstrates that drug release can in principle be controlled and tailored towards the given application, by manufacturing FGM with smoothly varying diffusivity properties. In particular, the model may be used as a computational tool by the pharmaceutical industry to reverse-engineer desirable FGM material properties and drug dosing to achieve a desirable drug release profile. As we move towards a future of precision medicine, tools that facilitate personalized drug delivery are becoming increasingly important.

We have also uncovered that, in general, the shape of the resulting drug release profiles cannot be obtained from a homogeneous material with a constant diffusivity. It is important to recognize that there are a number of limitations present in this work. Firstly, drug delivery often involves complex interactions between many physical, chemical and biological processes in addition to diffusion, which may in general also be concentration and/or time dependent. More effort is required to

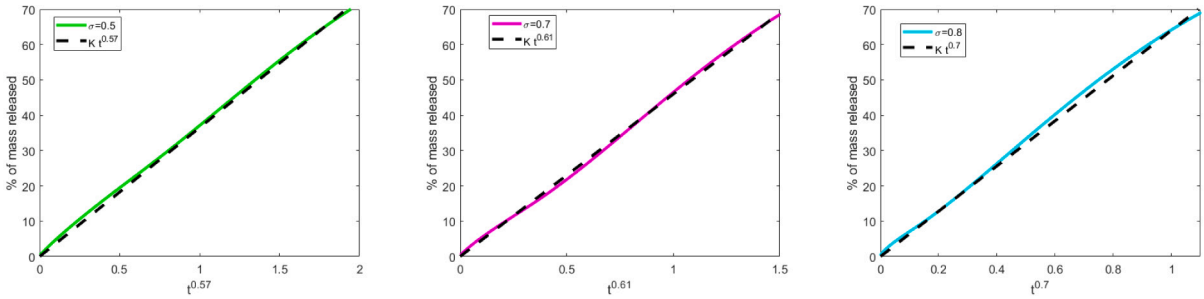

Fig. 10. Release curves P_r for logistic law (2.13) with $\lambda = 50$ and $\sigma = 0.5, 0.7, 0.8$ drawn vs t^β and related linear curves with $P_r = Kt^\beta$ parameters reported in Table 3.

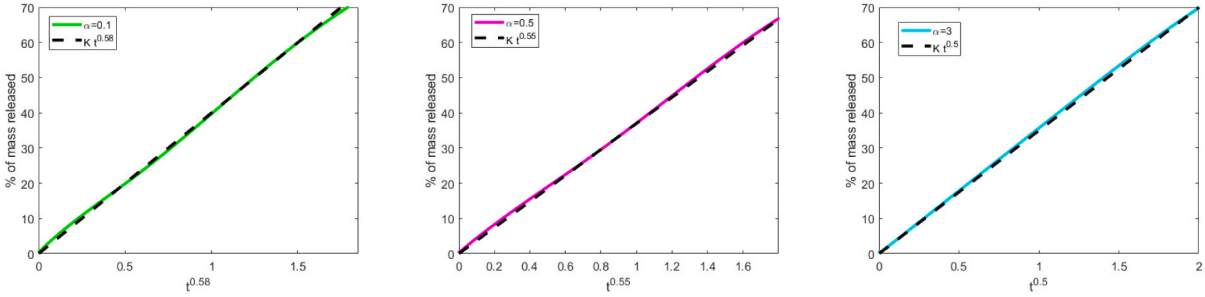

Fig. 11. Release curves P_r for power-law (2.6) with $\alpha = 0.1, 0.5, 3$ drawn vs t^β and related linear curves of the form $P_r = Kt^\beta$ with parameters reported in Table 3.

Table 3
Parameter fitting for K and β assuming $P_r = Kt^\beta$ for logistic and power-law release curves.

	Parameters	K	β
logistic (2.13)	$\lambda = 50, \sigma = 0.5$	36.5	0.57
	$\lambda = 50, \sigma = 0.7$	46	0.61
	$\lambda = 50, \sigma = 0.8$	64	0.7
power-law (2.6)	$\alpha = 0.1$	40	0.58
	$\alpha = 0.5$	37	0.55
	$\alpha = 3$	35	0.5

build in these additional complexities and assess their influence on drug release. A simple typical in-vitro scenario is modelled here: future work should couple a model of drug release from the DDD with the biological environment. Despite these limitations, this work serves as proof-of-concept, motivating the design of FGM with smoothly and continuously varying diffusivity properties. We hope and expect that this work will inspire experimental feasibility testing and validation of the ideas and models presented here.

Declaration of competing interest

The authors declare that they have no known competing financial interests or personal relationships that could have appeared to influence the work reported in this paper.

Data accessibility

All data supporting this study are provided within the main text.

Acknowledgements

Funding by Italian MIUR project "3D-Phys" (Grant No. PRIN 2017 PHRM8X) is greatly acknowledged. Dr. Sean McGinty and Dr. Gabriella Bretti acknowledge funding from the Royal Society (Grant number IEC\R2\222058).

References

[1] Y. Zhang, H.F. Chan, K.W. Leong, Advanced materials and processing for drug delivery: the past and the future, Adv. Drug Deliv. Rev. 65 (2013) 104–120.
[2] D. King, S. McGinty, Assessing the potential of mathematical modelling in designing drug-releasing orthopaedic implants, J. Contr. Rel. 239 (2016) 49–61.
[3] A.S. Timin, D.J. Gould, G.B. Sukhorukov, Multi-layer microcapsules: fresh insights and new applications, Exp. Op. Drug Deliv. 14 (5) (2017) 583–587.
[4] S. De Koker, R. Hoogenboom, B.G. De Geest, Polymeric multilayer capsules for drug delivery, Chem. Soc. Rev. 41 (2012) 2867–2884.
[5] N. Kumar Patra, et al., Nano based drug delivery systems: recent developments and future prospects, J. Nanobiotechnology (2018) 16:71.
[6] M. Grassi, G. Lamberti, S. Cascone, G. Grassi, Mathematical modeling of simultaneous drug release and in vivo absorption, Int. J. Pharm. 418 (2011) 130–141.
[7] J. Siepmann, F. Siepmann, Modeling of diffusion controlled drug delivery, J. Contr. Rel. 161 (2) (2012) 351–362.
[8] D.Y. Arifin, L.Y. Lee, C.H. Wang, Mathematical modeling and simulation of drug release from microspheres: implications to drug delivery systems, Adv. Drug Deliv. Rev. 58 (2006) 1274–1325.
[9] B. Kaoui, M. Lauricella, G. Pontrelli, Mechanistic modelling of drug release from multi-layer capsules, Comput. Biol. Med. 93 (2018) 149–157.
[10] E.J. Carr, G. Pontrelli, Modelling mass diffusion for a multi-layer sphere immersed in a semi-infinite medium: application to drug delivery, Math. Biosci. 303 (2018) 1–9.
[11] I.M. El-Galy, B.I. Saleh, M.H. Ahmed, Functionally graded materials classifications and development trends from industrial point of view, SN Appl. Sci. 1 (2019) 1378.
[12] J. Majumder, T. Minko, Multifunctional and stimuli-responsive nanocarriers for targeted therapeutic delivery, Exp. Opin. Drug Deliv. 18 (2) (2021) 205–227.
[13] G. Pontrelli, G. Toniolo, S. McGinty, D. Peri, S. Succi, C. Chatgilialoglu, Mathematical modelling of drug delivery from pH-responsive nanocontainers, Comput. Biol. Med. 131 (2021) 104238.
[14] X. Wu, Y. Zhu, Heterogeneous materials: a new class of materials with unprecedented mechanical properties, Mater. Res. Lett. 5 (8) (2017) 527–532.
[15] R. Madan, S. Bhowmick, A review on application of FGM fabricated using solid-state processes, Adv. Mater. Process. Technol. 6 (3) (2020) 608–619.
[16] J.H. Kim, G.H. Paulino, Finite element evaluation of mixed-mode stress intensity factors in functionally graded materials, Internat. J. Numer. Methods Engrg. 53 (2002) 1903–1935.
[17] B. Saleh, J. Jiang, R. Fathi, T. Al-hababi, Q. Xu, L. Wang, D. Song, A. Ma, 30 Years of functionally graded materials: an overview of manufacturing methods, applications and future challenges, Composites B 201 (2020) 108376.
[18] Y. Shinohara, Functionally graded materials, in: Handbook of Advanced Ceramics, second ed., 2013.
[19] J.M. Lowen, J.K. Leach, Functionally graded biomaterials for use as model systems and replacement tissues, Adv. Funct. Mater. 30 (44) (2020) 1909089.

[20] A. Zimmerling, Z. Yazdanpanah, D.M.L. Cooper, J.D. Johnston, X. Chen, 3D printing PCL/nHA bone scaffolds: exploring the influence of material synthesis techniques, Biomat. Res. 25 (3) (2021).
[21] D. Aregba-Driollet, F. Diele, R. Natalini, A mathematical model for the sulphur dioxide aggression to calcium carbonate stones: Numerical approximation and asymptotic analysis, SIAM J. Appl. Math. 64 (5) (2004) 1636–1667.
[22] J.C. Strikwerda, Finite Difference Schemes and Partial Differential Equations, SIAM, 2004.
[23] G. Pontrelli, F. de Monte, Mass diffusion through two-layer porous media: an application to the drug-eluting stent, Int. J. Heat Mass Transfer 50 (2007) 3658–3669.
[24] S. McGinty, G. Pontrelli, A general model of coupled drug release and tissue absorption for drug delivery devices, J. Contr. Rel. 217 (2015) 327–336.
[25] J. Crank, The Mathematics of Diffusion, second ed., Oxford Sci. Pub., 1980.
[26] P.L. Ritger, N.A. Peppas, A simple equation for description of solute release I. Fickian and non-Fickian release from non-swellable devices in the form of slabs, spheres, cylinders or discs, J. Contr. Rel. 5 (1987) 23–36.